Experimental Characterization of VAWT Airfoils Under Turbulent Flows

Carbo Molina, Andreu; Van de Maele, Sander Geert; Bartoli, Gianni; Runacres, Mark; De Troyer, Tim

Published in:
Wind Energy Exploitation in Urban Environment

DOI:
10.1007/978-3-030-13531-7_2

Publication date:
2019

Document Version:
Accepted author manuscript

Experimental characterization of VAWT airfoils under turbulent flows

Andreu Carbó Molina[1,2], Sander Van de Maele[2], Gianni Bartoli[1], Tim De Troyer[2] and Mark Runacres[2]

[1] Dept. of Civil and Environmental Engineering, Università degli Studi di Firenze, Via di Santa Marta 3, 50139, Firenze, Italy
[2] Thermo and Fluid Dynamics (FLOW), Vrije Universiteit Brussel, Pleinlaan 2, 1050 Brussels, Belgium
andreu.carbo.molina@dicea.unifi.it

Abstract. Vertical-Axis Wind Turbines are receiving the attention of the wind energy community for urban wind harvesting. However, their practical application is still far from maturity, due to the lack of understanding of urban flows. High turbulence is one of the main characteristics of wind in complex environments, so special attention has been paid to modelling it inside wind tunnels for prototype testing. Previous experiments showed a considerable boost in VAWT performance when turbulence intensity increases, but the explanation of this increase still has to be determined. This study analyses the effect of turbulent flows on the performance of a NACA0018 airfoil, using a blade model provided with pressure tabs and a traverse system to analyze the wake. The model is subjected to the same angles of attack and Reynolds numbers that would be found in normal VAWT operation, while turbulence intensity and integral length scale are kept at levels similar to those found in urban environments. The effect of turbulence is evident as it considerably delays the stall angle of the blade. Using a Single Streamtube model, the results from this parametric study are compared with the overall turbine ratings, in order to find a way to optimize turbine blades using a simplified set-up.

Keywords: VAWT, Urban flows, Airfoils, Turbulence

Nomenclature

b	Grid bar width [m]
c	Blade chord [m]
C_D	Drag coefficient [-]
C_L	Lift coefficient [-]
C_N	Normal force to the blade coefficient [-]
C_p	Pressure coefficient [-]
C_P	Turbine power coefficient [-]
C_{Psf}	Turbine power coefficient in smooth flow (low turbulence) [-]
d	Distance to grid [-]
D	Drag [N]

I_u	Turbulence intensity in the flow direction [%]
L_{ux}	Integral length scale of turbulence in the flow direction [m]
P	Pressure [Pa]
Re_c	Chord Reynolds number [-]
u	Local wind speed in the flow direction [m/s]
U	Incident wind speed in the blade/turbine [m/s]
x	Distance along the blade chord [m]
α	Angle of attack [˚]
δ	Uncertainty
λ	Tip-speed ratio [-]
ρ	Air density [Kg/m^3]
θ	Azimuthal angle [˚]
HAWT	Horizontal-Axis Wind Turbines
SST	Single Streamtube
rms	Root mean square
VAWT	Vertical-Axis Wind Turbines

1 Introduction

During the last years, harvesting the urban wind resource has become an objective for the wind energy community [1]. Placing small turbines on the roofs of high buildings would allow reaching large heights while saving the cost of tower constructions, and at the same time promote on-site consumption avoiding energy transport losses [2]. Contrary to the general trend, Vertical-Axis Wind Turbines (VAWT) have been considered as a viable alternative to conventional horizontal-axis ones for urban wind harvesting [3]. Although their efficiency is lower, their omnidirectionality and lower rotational speeds allow them to adapt better and be less noisy under the highly turbulent flows present in urban environments [4]. Among the variety of VAWT designs, H-Darrieus turbines have been selected for this research, as their higher efficiency and simple geometry make them the option with the highest potential [5].

Operation of wind turbines in urban environment is, however, not straightforward. Due to the increased terrain roughness (buildings, infrastructures…) the atmospheric boundary layer is shifted upwards in the cities, resulting in significantly lower wind speeds [1]. This flow is, furthermore, very complex, exhibiting high variability in wind speed and incidence angles that make the positioning of the turbine and its energy yield prediction a complicated issue [6].

All those features contribute to increase the level of turbulence of the flow, which makes that in urban environments the average turbulence vales are significantly higher (I_u > 10%) than those in open terrain [7]. Turbulence is not often considered in the design process of VAWTs, and the study of its effect in the turbine's performance is limited to on-field data with the wind turbulence measured by a nearby meteorological station. The impossibility to control all external conditions make the results from those studies not definitive, offering contradictory results between them [8 - 10].

Wind tunnel experiments could be used to isolate the effect of turbulence from other parameters in order to provide precise and repeatable turbine ratings. However, few difficulties have to be tackled first: common experimental facilities have very low background turbulence (I_u < 1%), and therefore this value should be augmented by the use of grids and other equipment. To date, few studies addressed the topic of turbulence [11, 12], with not enough data available to support solid conclusions.

An experimental set-up, presented in the last TUrbWind Conference [13], was developed within a collaboration between the University of Florence and the Vrije Universiteit Brussel to model urban flows in the wind tunnel. The optimization of turbulence grids allowed to study the effect of turbulence intensity on the mechanical power generated by a H-Darrieus VAWT. The results showed a considerable increase in turbine performance for moderate turbulence levels. Understanding the nature of this power increase could help to develop a new generation of more efficient Urban Wind Turbines.

A study on the near wake revealed that turbulence promoted faster wake recovery and reduced the losses caused by the shaft [14]. However, the main candidate to justify the performance increase is the impact of turbulent flows in the stall of the blades [3]. Hoffman in 1991 already detected positive influence of turbulence in the Cl-alpha curve of a symmetric NACA0015 airfoil [15]. And the subject has been studied in detail for non-symmetrical HAWT airfoils, always resulting in a very positive influence of turbulence on the stall of the airfoils [16 - 17]. But none up to the moment combined the characteristics of the airfoils with the overall VAWT performance measured under different turbulence flows. The objective of this work is to establish a relationship between the overall behavior of the turbine and the effect on the airfoils of different flows, in order to set a benchmark that would allow to optimize the performance of urban VAWTs with a more simplified set-up.

2 Methodology

2.1 Wind tunnel settings

The facility

The research is performed at the Vrije Universiteit Brussel, in Belgium. The boundary layer wind tunnel has a length of 11 m that allows to develop stable turbulence intensity and length scale levels before the test section. The test section, with 1.04 m of height and 2 m width, permits testing scaled buildings and small wind turbines. Fig. 1 shows the wind tunnel interior with the turbulence grid.

Fig. 1. VUB low speed wind tunnel with turbulence grid.

Measurement techniques

Pressure measurements on the blade taps are performed using a Scanivalve ZOC33 electronic pressure scanner equipped with 16 channels. It has a full scale range of 2.5 kPa, providing an accuracy of 0.15% of this range (approximately 3.7 Pa). The sampling frequency for the pressure tabs data is 10 Hz, as high time resolution is not required, and 30 seconds are sampled to reduce the random error.

The wind flow characteristics are measured with a Constant Temperature Hot-Wire Anemometer, model Dantec mini-CTA 54T42. Its calibration is done using a Pitot tube. The time histories obtained from the hot-wire are acquired by a National Instruments Card and processed using Labview software to obtain the mean speed and turbulence levels. To register the wind speed of the wake, the hot wire is mounted 1 chord downstream in a traverse system controlled by Arduino. As hot wire allowed us to obtain higher resolution in frequency, the samples were taken at 1 kHz, with also 30s of measurement.

The turbulence intensity was calculated as usual by using the root mean square (*rms*) and the incoming longitudinal flow speed (Eq. 1), while the longitudinal integral length scale L_{ux} was calculated according to Taylor's frozen-eddy hypothesis.

$$I_u = \frac{u_{rms}}{U} \tag{1}$$

Generation of turbulent conditions

A squared-mesh wooden grid (Fig. 1) is placed upstream of the model to generate different levels of turbulence intensity (I_u) and integral length scale (L_{ux}), following the recommendations by Lanneville (Eq.2) and Roach (Eq. 3) [19, 20]:

$$I_u = 2.58\left(\frac{d}{b}\right)^{-8/9} \quad (2)$$

$$L_{ux} = 0.2b\left(\frac{d}{b}\right)^{1/2} \quad (3)$$

Where d is the distance to the grid and b the bar size. The profiles obtained by moving the grid upstream and downstream are enounced in Fig. 2. The power delivered to the wind tunnel fan is modified in order to obtain a similar wind speed in all cases. It can be observed how the uniformity of the values is maintained over the height of the wind tunnel (the most limiting dimension), to be able to obtain a clear indication of the influence of turbulence. In fact, Fig. 2 represents the profiles under which the VAWT performance was measured (U = 8 m/s), while to obtain the same Re_c values in the airfoil other wind speeds were used. However, the I_u and L_{ux} remained not affected by the different wind speeds. This and other details of the procedure of the building of the grid and the obtention of the profiles can be consulted at [13].

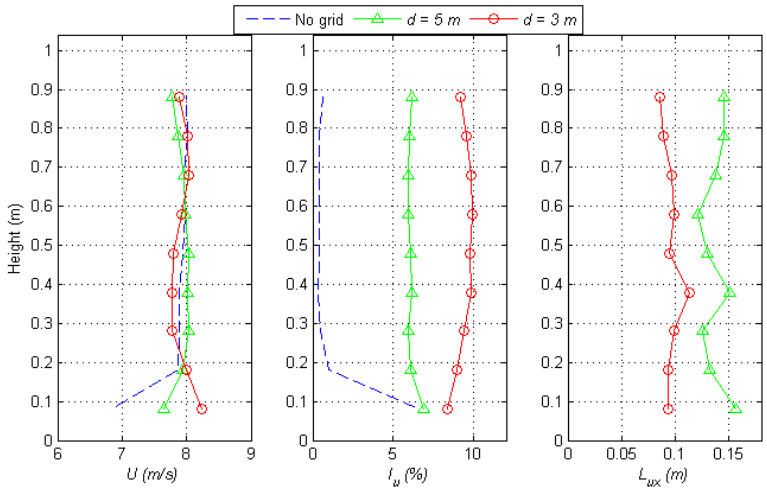

Fig. 2. Wind speed and turbulence profiles obtained with the different positions of the grid.

The average values obtained with the grid positions are enounced in Table 1.

Grid position d	No grid	5 m	3 m
Mean windspeed U	7.94 m/s	7.97 m/s	7.90 m/s
Mean I_u	0.45 %	6.00 %	9.58 %
Mean L_{ux}	-	0.136 m	0.096 m

Table 1. Mean flow values obtained in the test section with the different grid positions.

2.2 Turbine prototype

The rotor is a two-blade H-type Darrieus turbine with two NACA0018 blades with a 5 cm chord (c) and two inclined struts per blade (see Fig. 3). Due to the small size of the rotor, angular speeds (and thus centrifugal loads) were high in order to achieve the suitable Reynolds numbers on the blades ($Re_c \sim 10^5$). To ensure proper mechanical properties, the rotors were manufactured using carbon-epoxy composite. Even when at low Reynolds numbers laminar separation is important no high-lift devices were added to the blade. Transition could be forced by e.g. transition strips, but preliminary tests with such strips on the VAWT did not give the expected result, so this avenue was not pursued further.

The VAWT rotor was connected via a torque sensor and a drive belt (with gear ratio 100/28) to a brushed-DC motor. This motor was used to drive the VAWT rotor during start-up, while acted as a generator in normal operation. The electrical output of the motor was fed to a circuit of variable resistance for angular speed control. A torque sensor was used to measure the mechanical torque and angular speed of the VAWT. The torque sensor, drive belt, DC motor, and measurement equipment were housed inside an aluminium frame. The torque sensor was a Lorenz Messtechnik DR-3000 sensor with an accuracy of $\pm 2 \cdot 10^{-3}$ Nm. It was fitted between two torsionally-stiff couplings to allow for possible misalignments.

Fig. 3. VAWT prototype in the wind tunnel.

2.3 Airfoil model

In order to obtain the Reynolds numbers of $1 \cdot 10^5$ within the windspeed range of the wind tunnel, a model was selected with a chord of 10 cm. The location of the pressure tabs was chosen from literature [21] (Table 2).

Tap	1	2	3	4	5	6	7	8	9	10	11	12	13
x (cm)	0.125	0.250	0.5	1	1.5	2	3	4	5	6	7	8	9

Table 2. Positions of pressure tabs along the chord of the airfoil model.

To ensure the desired structural properties, the blade was made by laminating fiberglass, using an aluminum mold to obtain the desired shape. The mold was manufactured with a CNC-milling machine using CAD-drawing and CAM-software by Autodesk Inventor. After the machining, the mold was polished by hand and finished with the use of a conventional mill.

In the first step of making the blade, fiberglass was laminated into the molds. The entire mold was cured inside a vacuum bag in order to prevent air bubbles. The pressure tabs were drilled into a brass tube positioned underneath the surface of the blade. The positioning of these tubes was critical, therefore jigs were made to hold the tubes in the correct place (Fig. 4).

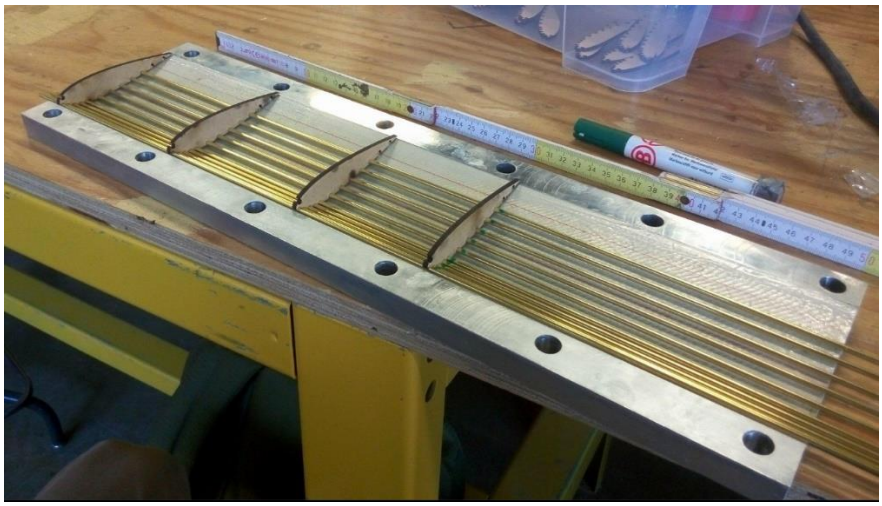

Fig. 4. Positioning of the tubes with the aid of jigs.

After all tubes were positioned, the mold was closed and both halves were glued to each other. In order to prevent buckling of the thin fiberglass skin, the model was filled with polyurethane foam.

The drilling of the pressure tabs was made with a fine 0.7 mm drill with the help of a drill guide to enhance hole precision. By using this method two rows of pressure tabs were drilled, with the idea that if one hole was oriented different than the other this would result in a different pressure reading. By using two holes this error would be averaged out.

The blade was clamped into an aluminum block for stiffness, and an end plate was glued on the block. The end plate on the other end of the model was already installed in the wind tunnel, and could not be adjusted in height. For this reason a platform was made with 4 bolts on which the model could be mounted. End plates were used to limit 3-D effects, so the flow could be considered 2D for simplicity in the calculations. Fig. 5 gives a clear overview of all components.

Fig. 5. Airfoil model overview, with end plates and traversing system.

2.4 Data analysis

Calculation of aerodynamic coefficients:

The differential pressure obtained from the pressure tab readings is used to calculate the pressure coefficient C_p for each position along the blade chord (Equation 4):

$$C_p = \frac{P - P_\infty}{\frac{1}{2}\rho U^2} \tag{4}$$

From here, the normal force (perpendicular to blade chord) coefficient is calculated by integrating the difference between the C_p in the upper and lower part of the blade (Equation 5):

$$C_N = -\int_0^1 \left(C_{P,up} - C_{P,low}\right) d\left(\frac{x}{c}\right) \tag{5}$$

Supposing low angles of attack ($\alpha < 20^{\circ}$) and $C_L > C_D$, the lift coefficient C_L can be approximated by (Eq. 6):

$$C_L = C_N cos\alpha \tag{6}$$

Drag is calculated by the wake survey method, or scanning transversally the wake of the profile. This method, based in the integral momentum conservation, permits calculating the forces acting on a body from their reactions on the flow. The model is limited due to its assumptions of constant static pressure and negligible turbulent and viscous stresses, but it simplicity makes it useful in this preliminary study. The formulation from Jones (Equation 7) will be used [22]:

$$D = \int \rho u(U - u)dy \tag{7}$$

Resulting in Equation 8:

$$C_D = \frac{D}{\frac{1}{2}\rho c U^2} \tag{8}$$

Streamtube modelling:

To extrapolate the obtained blade coefficients into the overall turbine performance, a single streamtube (SST) model as in [3] is used. This simple model was first developed by Templin [23] to calculate the aerodynamical performance of a curved-blade Darrieus, but has been adapted for the H-rotor as in Fig. 6 [24]. It is based in the actuator disk theory, assuming the induced velocity is the same in both faces of the turbine.

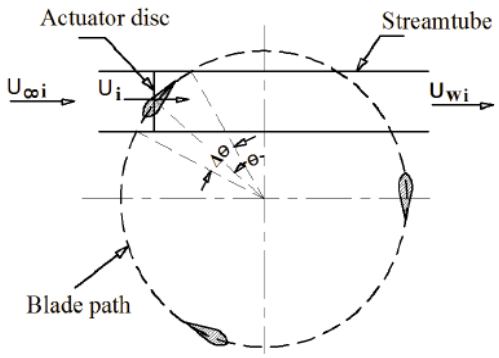

Fig. 6. 2D schematic of the streamtube model [24].

The code delivers reasonable results given its simplicity, although it fails to describe accurately the stall region [3]. This is not a major inconvenience as the study focuses in the optimal point of operation of the turbine, where blades are mostly not

stalled. In our case, the overall performance is highly overpredicted, as the code does not account for shaft, struts and tip losses, or mechanical friction. But the matter of interest is to determine if it is able to describe the differences in turbine performance caused by increased turbulence, as the main inputs of the code are the C_L and C_D curves of the blades.

Uncertainties calculation:

Uncertainties are calculated by the error propagation method, enounced in Eq. 9 [20]:

$$\delta_R = \sqrt{\sum_i^N \left(\frac{\partial R}{\partial x_i}\delta_{xi}\right)^2} \tag{9}$$

The error in the power curves is explained in [13], and increases with turbulence as the wind speed profile uniformity descends.

For the measurements obtained with the pressure tabs in the airfoil, several contributions are analyzed. As the sampling time was set long enough to minimize sampling error, the uncertainties contributions were determined after the accuracy after the different measurement equipment. These errors range from under 5% in high pressure points, low turbulence wind, to 15% at low pressure points in the presence of high turbulence flow. The main error sources are:

- Accuracy of the pressure transducer (3.7 Pa)
- Uncertainty in the measured wind speed: in which contributes pitot sensitivity (4 Pa) and wind profile uniformity (depending of I_u).

For the wake survey measurements, the uncertainty in wind speed is the most limiting factor, as the positioning system precision is very accurate. In percentage, the uncertainty is the order of 20% in the laminar zone, due to the low values, while in stall this calculated error is the order of 5%.

These error values are relatively high, but difficult to reduce with the available equipment. However, the results are still considered meaningful. For simplicity in the presentation of data, only some error bars will be presented as illustrative examples.

3 Results

3.1 Turbine power curves

Fig. 7 presents the power curves around the maximum efficiency obtained with the VAWT model in the turbulence conditions presented in Table 1. Due to confidentiality reasons, the values were normalized by the maximum C_P obtained under smooth flow conditions. It is evident that the increased I_u provided a notable increase of the turbine performance, up to +30% for the higher turbulence case, while the increase for medium turbulence levels is around 17%. This increase is more evident for lower λ, when a larger part of the rotation occurs under stalled conditions. The curves also show a displacement of the optimal λ upon lower values when turbulence is increased.

The following sections will try to analyze until which point this behavior depends in the performance of the blade under turbulence flows.

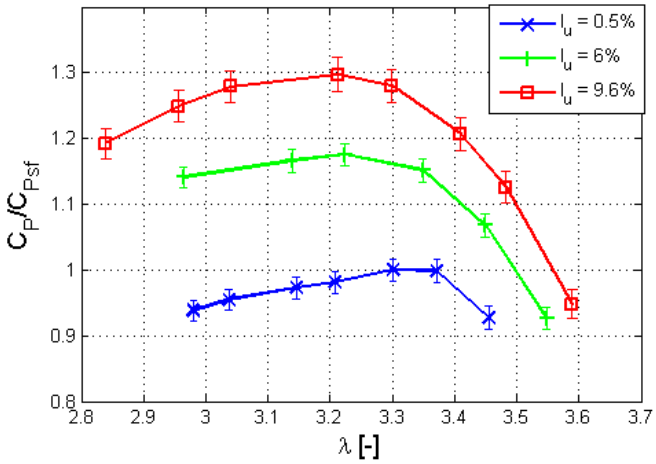

Fig. 7. Power curves obtained with the VAWT under different turbulence conditions, normalized with the optimum C_P in smooth flow.

3.2 Airfoil measurements

The conditions for the airfoil measurements are selected from the SST results. Fig. 8 presents the expected values of α and Re_c that the blade encounters along one rotation at around the optimum point of operation (λ = 3.3). It can be seen how at $\theta = 0^\circ$ the blade, facing the flow, reaches the maximum Reynolds number but at a zero α. Minimum Re_c is obtained at the opposite side of the rotation, while during the rest of the rotation the wind reaches the blade with an angle of attack, varying from -11˚ to +11˚ approximately.

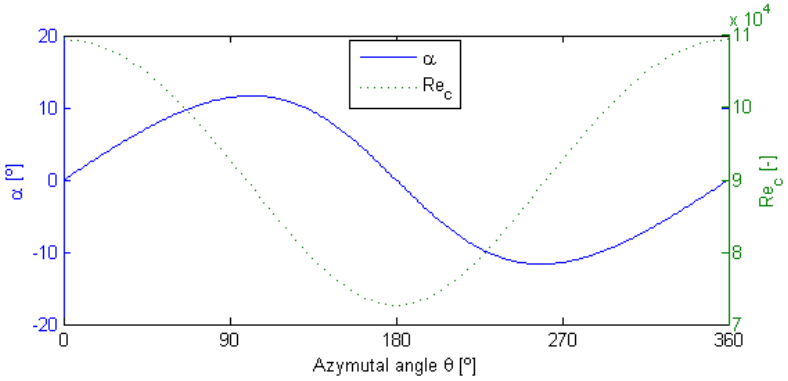

Fig. 8. Values of α and Re_c encountered by the blade along a rotation at λ = 3.3, calculated with the SST.

Considering this, and the various limitations (set-up, structural, time), a set of test conditions was selected (Table 3). Two values of Reynolds are selected: $8 \cdot 10^4$ to compare with literature and 10^5 because it is more similar to the values shown at Fig. 8. Those Reynolds values are low in comparison to large wind turbines, but in the same order of magnitude of the small VAWTs that can be found in urban environments. Being the NACA0018 a symmetrical airfoil, only positive α are considered.

Reynolds numbers Re_c	$8 \cdot 10^4$ and $1 \cdot 10^5$
Angle of attack α	0 to 20º
Turbulence intensity I_u	0.5%, 6.0% and 9.6%

Table 3. Test conditions for the airfoil measurements.

Fig. 9 and Fig. 10 present the C_L and C_D curves obtained with the different Reynolds and turbulence conditions presented in Table 3, compared with literature data collected in the Sandia project [26] in a low-turbulence wind tunnel facility. It can be seen how the lift curve obtained at I_u = 0.5% coincides with the literature one for angles of attack lower that 12º, while afterwards the registered lift value is significantly higher than in literature. Considering the drag coefficient, the values obtained with the wake survey method are considerably higher than the ones from literature. For low angles this can be attributed to the finishing of the model, while for high α the high values can be explained by the difference in the experimental methodology. The Jones method, presented in section 2.4, is of limited use for stall conditions as neglects viscous and turbulence effects, while the measurements in [26] were performed with an aerodynamic balance. However, the focus of this study was to compare between the different turbulence levels, and in those cases all measurements have been obtained with the same methodology. Examples of the error bars for each curve at $Re_c = 80 \cdot 10^3$ are also presented.

When comparing between the different flow conditions, it can be appreciated how Re_c exerts a positive effect both in C_L and C_D, however it is only considerable with the low turbulence case (minimum in the others). On the other hand, the effect of I_u in the polar curves is evident. Although there is a slightly higher C_L slope for small angles in the low turbulence case, it can be appreciated how the effect of turbulence is basically a large delay of the stall, as predicted in literature [3, 17]. When increasing the turbulence, the stall is later and smoother, while the maximum values of C_L remain generally constant (but occur also at higher α).

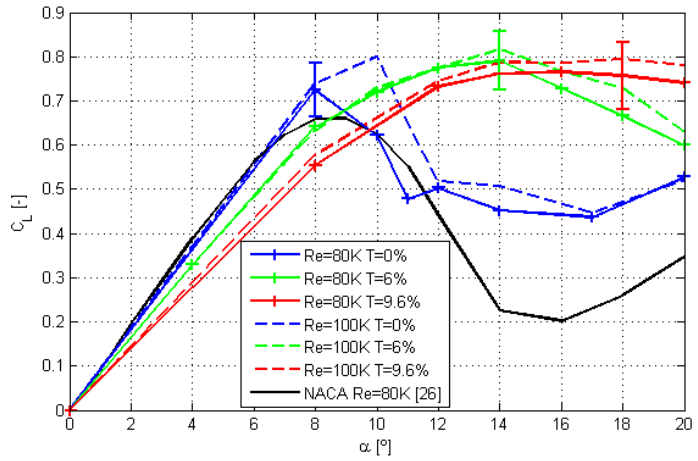

Fig. 9. C_L- α curves obtained with different Re_c and I_u conditions, compared with literature data [26].

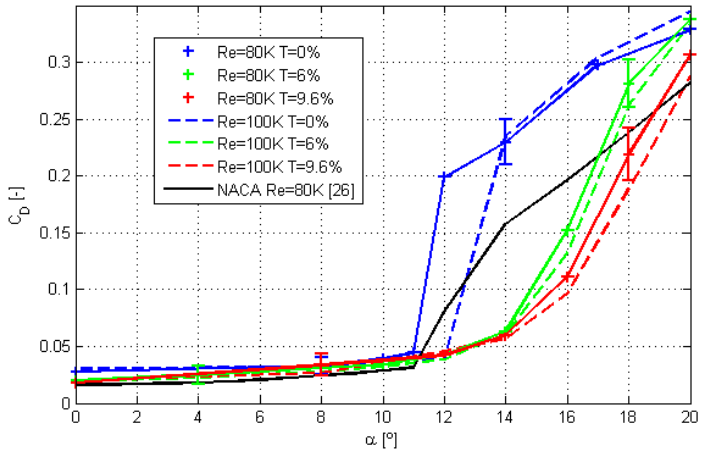

Fig. 10. C_D- α curves obtained with different Re_c and I_u conditions, compared with literature data [26].

The pressure taps set-up also allowed to measure the local pressure along the blade chord. It is interesting to see how the pressure distribution is affected by the turbulence increase. Fig. 11, Fig. 12 and Fig. 13 present the normalized pressure distribution along the blade at $\alpha = 8^\circ$, $\alpha = 14^\circ$ and $\alpha = 20^\circ$. The C_p values are inverted so the suction side distribution appears at the top. At 8°, still in the linear phase, it can be seen how the distribution is similar in the 3 cases, just with slightly higher pressure in the low turbulence case. Fig. 12 at 14° shows how the blade at low turbulence is completely stalled, while, in this case, the two turbulent cases are still lifting (even more

than at $\alpha = 8^{\circ}$), and nearly with exact values between them. At 20˚, in all three conditions the blade appear stalled, except for the high turbulence case, where near the leading edge there is still some suction in the upper part of the blade. Therefore, it can be concluded that the effect of I_u is that, instead of a sudden detachment of the flow in all the blade, in turbulent flow the detachment occurs progressively from the trailing to the leading edge as α increases. Those results show perfect agreement with the C_L and C_D values in Fig. 9 and Fig. 10.

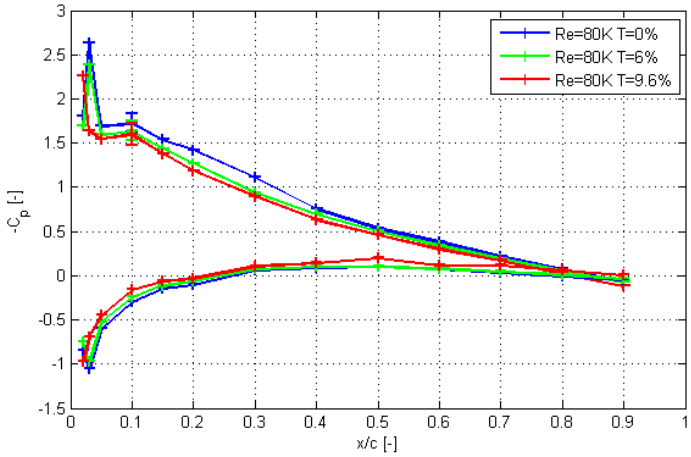

Fig. 11. C_p coefficients measured along the chord with different I_u conditions at $\alpha = 8^{\circ}$.

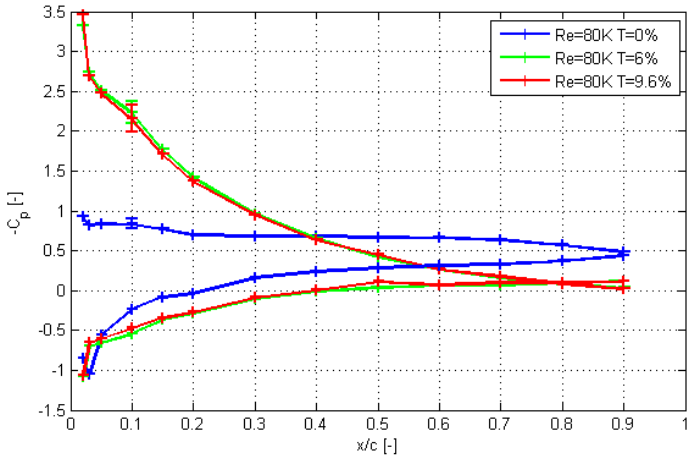

Fig. 12. C_p coefficients measured along the chord with different I_u conditions at $\alpha = 14^{\circ}$.

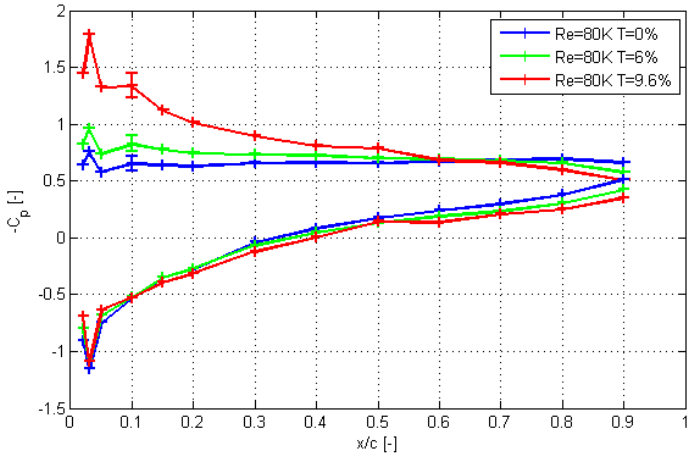

Fig. 13. C_p coefficients measured along the chord with different I_u conditions at $\alpha = 20^{\circ}$.

3.3 VAWT performance prediction using single streamtube model

As stated in section 2.4, the limitations of the SST prevent obtaining realistic values in the C_P curves. Moreover, because of time limitations the curves are only available for two Re, therefore limiting very much the accuracy. So the results observed in Fig. 14 are only a first approximation of the potential of the technique. Comparing it with Fig. 7 it is clear that the curve for smooth flow decays too fast when encountering blade stall, while in the turbulent cases stall does not occur in any moment and the curves are much less pronounced. This fact can be explained because of the lack of data, but mostly because the dynamic stall is not considered. However, even with the simplicity of the model, it is remarkable how the optimal λ is accurately predicted: around 3.2, and slightly lower as turbulence is increased.

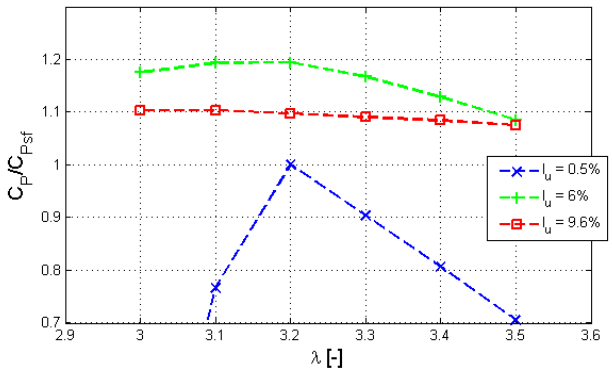

Fig. 14. Power curves (normalized with the max. C_P in smooth flow) obtained by introducing C_L and C_D curves in the SST model.

The increase of peak performance is also accurately described for the medium turbulence case (20% against 19%), but in this case the highest turbulence case presents intermediate values. This is clearly appreciated in Fig. 15 where the max C_P obtained with the SST code is compared with the experimental case. The reason of this differences for high turbulence can be found in the limitations of the model, which does not consider dynamic stall neither the effect of the shaft, two factors in which it was proven that the increase of turbulence had a positive influence in VAWT performance [3, 14, 17]. Therefore, the model should be further improved to be able to predict accurately the performance of a VAWT for high turbulent cases.

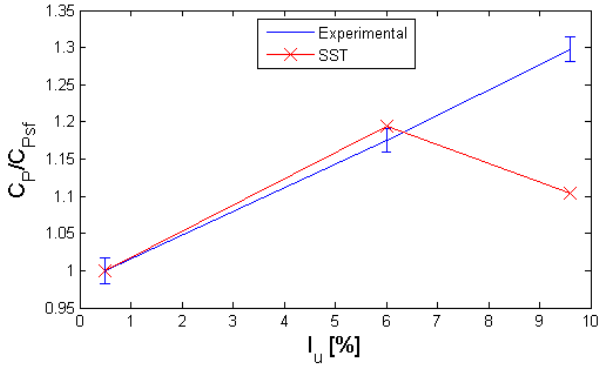

Fig. 15. C_{Pmax} evolution with incoming I_u, for VAWT tests and SST modelling. Normalized with the C_P obtained in the smooth flow case.

4 Conclusions

The study proposed a set-up that would allow to optimize VAWTs for turbulent flows. Following previous studies and literature, it was shown that the using passive grids turbulent conditions could be generated inside the wind tunnel. Under those conditions, a small H-Darrieus VAWT was tested, revealing a power increase due to turbulence at low Reynolds numbers. Aiming to relate those results to the blade aerodynamics, a NACA0018 blade provided with pressure tabs was built to observe the evolution of pressure distribution in the different turbulent conditions.

C_L curves obtained with this method present good agreement with existing literature, and show that the main effect of turbulence is an increase of the stall angle. At a Re_c number of $80 \cdot 10^3$, the stall angle of a NACA0018 at low turbulence (I_u = 0.5%) is around 11˚, while for medium values (I_u = 6%) the stall angle happens over 16˚, and for higher values (I_u = 9.6%) the blade stalls smoothly after 18˚. The pressure distributions also showed that as turbulence increase this stall is much less pronounced, with the detachment of the flow occurring progressively towards the leading edge as α increases. On the other hand, for low angles of attack C_L was slightly higher at low turbulence, while its maximum value overall was similar in all turbulent cases (just happening at different α).

C_D curves obtained with the wake survey method tended to overestimate the vales from literature, a fact that can be caused by the different methodology and due to the roughness of the model. In general the stall angles were correctly predicted, and it was found that the maximum values of C_D (after stall) were also similar between all turbulent cases. It is also worth noticing that the effect of Reynolds was lower as turbulence increases.

Even when the airfoil curves suggested a substantial increase of performance with turbulence (as measured with the turbine prototype in previous work), the first try to model this performance numerically was not successful. Introducing the experimental polar curves into a Single Streamtube code detected the rise of C_{Pmax} for medium turbulence increases (I_u from 0.5% to 6%), but was not able to describe accurately the case with higher turbulence. The influence of dynamic stall and the turbine shaft, that were not considered but in which turbulence exerts a significant effect, are the main suspects for this discrepancy.

4.1 Future developments

This work represented only the first step into finding a way to predict more accurately the effect of turbulence in VAWT performance. Therefore, the continuation of the work will be devoted into improving the accuracy of the method.

Experimentally, the measurements can be recreated at more Reynolds numbers and different values of turbulence. A set-up with oscillating blade like in Amandolèse [17] would allow obtaining the curves with the dynamic stall effects. It will be interesting also to double-check the measurements with an aerodynamic balance, specially to explain the difference against literature data in values after stall.

The numerical code, also, was revealed too simple to describe accurately the behavior of the whole turbine. The use of more refined codes (like multiple streamtube [3]) or CFD modelling, and including the effect of the shaft is recommended to try to obtain better agreement with experimental results.

References

1. Mertens, S.: Wind Energy in the Built Environment. Brentwood: Multi-Science (2006).
2. Barlow, J. F., Drew, D. R.: Wind flow in the urban environment. From WINERCOST Work-shop ‘Trends and Challenges for Wind Energy Harvesting’, pp. 15-24. Coimbra, Portugal, (2015).
3. Paraschivoiu, I.: Wind turbine design: with emphasis on Darrieus concept. Monreal: Presses inter Polytechnique (2002).
4. Bianchini, A., Ferrara, G. and Ferrari, L.: Design guidelines for H-Darrieus wind turbines: Optimization of the annual energy yield, Energy Conversion and Management 89 690-707 (2015).
5. Aslam Bhutta M. M., Hayat, N., Farooq, A. U., Ali, Z., Jamil, S. R., Hussain Z.: Vertical axis wind turbine - A review of various configurations and design techniques. Renewable and Sustainable Energy Reviews 16 (4), 1926-1939, (2012)

6. Bianchi S., Bianchini A., Ferrara, G., Ferrari, L.: Small wind turbines in the built environment: influence of flow inclination on the potential energy yield. J Turbomach 136 (2014)
7. Janajreh, I., Su, L., Alan, F.: Wind energy assessment: Masdar City case study. Renewable Energy 52, 8-15 (2013).
8. Bertényi T., Wickins, C., McIntosh, S.: Enhanced energy capture through gust-tracking in the urban wind environment. 48th AIAA Aerospace Sciences Meeting Including the New Horizons Forum and Aerospace Exposition. Orlando, Florida. (2010).
9. Pagnini, L. C., Burlando, M., Repetto, M. P.: Experimental power curve of small-size wind turbines in turbulent urban environment. Applied Energy 154 (2015).
10. Lee, K. Y., Tsao, S. H., Tzeng, C. W., Lin, H. J.: Influence of the vertical wind and wind direction on the power output of a small vertical-axis wind turbine installed on the rooftop of a building. Applied Energy 209 (2018).
11. Miau, J. J., Huang, S. W., Tsai, Y. D., Liang, S. Y., Hsieh, C. H., Chen, S. J., Hu, C. C., Cheng, J. C., Leu, T. S.: Wind tunnel study on aerodynamic performance of small Vertical-Axis wind turbines. Cheng Kung University, Taiwan (2012).
12. Ahmadi-Baloutaki, M., Carriveau, R., Ting, D. S. K.: Performance of a vertical axis wind turbine in grid generated turbulence. Sustainable Energy Technologies and Assessments 11 (2015).
13. Carbó Molina, A., Bartoli, G., De Troyer, T.: Generation of Uniform Turbulence Profiles in the Wind Tunnel for Urban VAWT Testing. In: Battisti L., Ricci, M. (eds) Wind Energy Exploitation in Urban Environment. TUrbWind 2017. Green Energy and Technology. Springer, Cham. (2018).
14. A Carbó Molina, A., Massai, T., Balduzzi, F., Bianchini, A., Ferrara, G., De Troyer, T., Bartoli, G.: Combined experimental and numerical study on the near wake of a Darrieus VAWT under turbulent flows. IOP Conf. Series: Journal of Physics: Conf. Series 1037 (2018).
15. Hoffmann, J. A.: Effects of freestream turbulence on the performance characteristics of an airfoil, AIAA Journal, Vol. 29, No. 9 (1991).
16. Devinant, P., Laverne, T., Hureau, J.: Experimental study of wind-turbine airfoil aerodynamics in high turbulence. Journal of Wind Engineering and Industrial Aerodynamics 90(6):689-707 (2002).
17. Amandolèse, X., Széchényi, E.: Experimental study of the effect of turbulence on a section model blade oscillating in stall. Wind Energy 7:267–282 (2004).
18. Maldonado, V., Castillo, L., Thormann, A., Meneveau, C.: The role of free stream turbulence with large integral scale on the aerodynamic performance of an experimental low Reynolds number S809 wind turbine blade. J. Wind Eng. Ind. Aerodyn. 142 (2015).
19. Laneville, A. Effects of turbulence on wind induced vibrations of bluff cylinders Ph.D. thesis, University of British Columbia. Vancouver, Canada (1973).
20. Roach, P. E.: The generation of nearly isotropic turbulence by means of grids. Int. J. of Heat and Fluid Flow 8(2) (1982).
21. Barlow, J. B., Rae, Jr. W. H.: Low-Speed Wind Tunnel Testing. 3rd ed. USA: John Wiley & Sons. 701. (1999).
22. Schlichting, H.: Boundary layer theory. McGraw Hill (1979).
23. Templin, R. J.: Aerodynamic Performance Theory for the NRC Vertical-axis Wind Turbine. National Research Council Canada, National Aeronautical Establishment (1974).
24. Biadgo, A. M., Simonovic, A., Komarov, D., Stupar, S.: Numerical and Analytical Investigation of Vertical Axis Wind Turbine. FME Transactions 41, 49-58 (2013).
25. Dénos, R.: Fundamentals of Data Acquisition and Processing. Course Note 171, von Karman Institute for Fluid Dynamics, (2005).

26. Sheldahl, R. E., Klimas, P. C.: Aerodynamic Characteristics of Seven Symmetrical Airfoil Sections Through 180-Degree Angle of Attack for Use in Aerodynamic Analysis of Vertical Axis Wind Turbines. Sandia National Laboratories energy report (1981).